Neutron Star Matter and Neutron Star Models

H. Heintzmann

Institut für Theoretische Physik der Universität Köln

W. Hillebrandt, M. F. El Eid, and E. R. Hilf

Institut für Kernphysik der Technischen Hochschule Darmstadt

(Z. Naturforsch. **29 a**, 933–946 [1974]; received January 16, 1974)

Various methods to study the ground state of neutron star matter are compared and the corresponding neutron star models are contrasted with each other. In the low density region $\varrho < 10^{14}$ gr cm^{-3} the nuclear gas is treated here by means of a Thomas Fermi method and the nuclei are described by the droplet model of Myers and Swiatecki. For $\varrho > 10^{14}$ gr cm^{-3} both standard Brueckner theory with more realistic interaction (one-boson-exchange) potentials and the semiphenomenological theory of Fermi liquids (together with the standard Reid softcore potential) are applied to neutron star matter. It is shown that while the high mass limit of neutron stars is hardly affected, some properties of lowmass neutron stars such as their binding depend sensitively on these refinements. Various tentative (but unreliable) extensions of the equation of state into high density regime $\varrho > 10^{15}$ gr cm^{-3} are investigated and it is shown that the mass limit for heavy neutron stars lies around 2.5 solar masses. It is further shown that a third family of stable (hyperon) stars is not forbidden by general relativistic arguments if there is a phase transition at high densities.

1. Introduction

The discoveries of radio pulsars [1] and x-ray sources in close binary systems [2] and particularly the unique radio-optical-x-ray and γ-ray pulsar in the crab nebula [3] have stimulated renewed interest in the final stages of stellar evolution. Today it is believed that an ordinary star can end its life in at least three different ways:

1) A white- (and later black-) dwarf star, if the final mass M does not exceed the Chandrasekhar limit ($M \cong 1.4\, M_\odot$).
2) A neutron star, if the final mass does not exceed a certain other limit which will be discussed below.
3) A (white or) black hole provided the final mass exceeds this latter limit.

Apart from these final states there might exist others e. g. hyperon stars.

A great number of authors have calculated the properties of neutron star matter and neutron star models including the composition and the equation of state at both low and high density [4–13], the cooling process and the problem of energy dissipation [14–20], the superfluidity of neutrons and protons [21, 22] and the possible existence of a neutronic quantum crystal [23].

Our motivation for reconsidering here neutron star matter and neutron star models is the following:

More realistic nuclear forces than used so far have been derived from meson theory which rely only on the experimentally measured coupling strengths and meson masses.

We consider model-extensions of the high density regime of neutron star matter such as a possible quantum crystal and different hadronic equations of state to study their effect on a possible third family of stable stars or effects of anisotropy.

We pay special attention to the equation of state at low densities to see how the minimum mass of a stable, bound neutron star is affected by the equation of state.

We try to analyse the effects of alternative theories of gravitation on the properties of neutron star models.

The present paper is divided into three main sections. In section two we will treat neutron star matter from a microscopic point of view and discuss limiting cases for the equation of state. In section three the macroscopic structure of neutron stars is studied and the fourth section tries to establish a link between theory and observation.

Reprint requests to Dr. W. Hillebrandt, Institut für Kernphysik der Technischen Hochschule Darmstadt, *D-6100 Darmstadt*, FRG, Schloßgartenstraße 9.

2. Neutron Star Matter

2.1. The Outer and Inner Crust

At "low" densities ($\varrho > 10^5\,\mathrm{g\,cm^{-3}}$) matter in its ground state and at zero temperature consists of Fe^{56} nuclei arranged in a lattice so as to minimize their coulomb interaction energy. As the matter density increases the electron chemical potential $\mu_e = m_e c^2 + E_f$ increases. Above $\varrho = 10^5\,\mathrm{g\,cm^{-3}}$ the electrons are essentially free and above $\varrho \cong 10^7\,\mathrm{g\,cm^{-3}}$ they are fully relativistic.

The inverse β-process becomes energetically favourable if the electron chemical potential exceeds the respective Q-value. With increasing mass density the equilibrium nucleus present in the lattice becomes progressively richer in neutrons. At the density $\varrho_2 = 4.65 \times 10^{11}\,\mathrm{g\,cm^{-3}}$ the nuclei are so neutron-rich that with further increase of the mass density a neutron gas component occurs. Matter consists then of nuclei embedded in a neutron gas and electrons penetrating the lattice. At a density ϱ_3 nuclei are no longer present; rather matter is a uniform mixture of electrons, protons and neutrons.

To derive the properties of the cold neutron star matter for the density regime below ϱ_3, i. e. both the outer crust, where there is no neutron gas component ($\varrho < \varrho_2$), and the inner crust ($\varrho_2 \leqq \varrho \leqq \varrho_3$) we start from the specific free energy

$$f = f(T, n_b; \boldsymbol{x}) \tag{1}$$

of the matter where n_b is the mean total baryon density, $n_b := N_b/V$, and $x := (n_n, n_e, n_p, n_N, A, Z)$ denotes the set of "internal" parameters of the system, namely the number densities of neutrons, electrons, protons, nuclei; A, Z being the mass and charge of a nucleus. The "internal" parameters come to their equilibrium value when the matter approaches thermal equilibrium. The constraints of this process are baryon conservation and charge neutrality. In other words, f has to be minimum for fixed n_b and T, i. e.

$$\partial_{\boldsymbol{x}}^{n_b, T} = 0\,. \tag{2}$$

We calculated the partial derivatives of f by numerical differentiation. Then the pressure P and the equation of state are determined by

$$P = P(n_b) = n_b\,\mu(n_b) - f(n_b)\,. \tag{3}$$

The chemical potential $\mu := \partial_{n_b} f$ can be plotted with equation (3) as a function of P namely

$$\mu(n_b) = \mu\big(n_b(P)\big) = \mu(P)\,. \tag{4}$$

To find f we imagine around each nucleus a unit cell (volume V_c) with a baryon density n_b and zero total charge. The nuclei (A, Z) are assumed to have spherical symmetry and a volume V_N.

The free energy density may then be written as

$$f = f_e(n_e) + [f(n_n, n_p) + f_{int}(n_n, n_p)]\,(1 - n_N V_N) + n_N B(A, Z, V_N, n_N)\,. \tag{5}$$

The factor $(1 - n_N V_N)$ is the fraction of the total volume V_c of the cell filled by the gases only. The first term in (5) is the free energy density (kinetic energy per volume) of the extreme relativistic, degenerate electron gas. As the electron Fermi wave number is relatively large ($k_f > 30\,fm^{-1}$) we assume, that the electrons completely penetrate the nuclei and have a uniform density over the whole system.

For $f_e(n_e)$ one has the relation

$$f(x) = \frac{{m_e}^4 c^5}{24\,\hbar^3 \pi^2}\{3\,x(1+x^2)^{1/2}(1+2\,x^2) - 8\,x^3 - 3\ln\left(x + (1+x^2)^{1/2}\right)\} \tag{6}$$

where

$$x := (3\,\pi^2 n_e)^{1/3}\,\hbar\,c/m_e c^2\,.$$

For the calculation of the second term of (5) we applied the Thomas-Fermi calculation of Weiss and Cameron [24], which is based on the V_α and V_γ nucleon potentials of Levinger and Simmons [25]. We used the result of the V_α-potential. In addition we took another set of interaction strength parameters to match the nuclear masses of the known nuclei. Specifically we used the V_α of Levinger and Simmons with $a_{se} = 8.2$ instead of 7.552, $a_{te} = 5.4$ (4.964), $a_{so} = -4.9$ (-4.479), and $a_{to} = 0.9$ (0.529).

We used also the Thomas-Fermi calculations given by Myers and Swiatecki [26] for homogenous nuclear matter to determine the potential energy of the neutron gas. These calculations are based on a more realistic potential than the V_α-potential of Weiss and Cameron.

The parameter of the two body potential of Seyler-Blanchard [26a] as used by Myers and Swiatecki are connected with the parameters of the Droplet-Model mass formula which we applied to desribe the binding energy of the neutron-rich nuclei. Finally the term $B(A, Z, n_N, V_N)$ in Eq. (5) is the binding energy of the nuclei including their lattice energy as follows:

The lattice energy is the energy of a regular Coulomb lattice of positively charged nuclei embedded in an uniform electron gas. We can take the lattice energy into account by adapting (kindly due to H. v. Groote, 1971) the Droplet-Model mass formula of Myers [26] to the given charge distribution in the unit cell as shown in Figure 1. The unit cell is now replaced by a sphere of the same volume (Wigner-Seitz method). The radius of the spere R_c is given by

$$R_c = (3/4\,\pi\, n_N)^{1/3}\,. \tag{7}$$

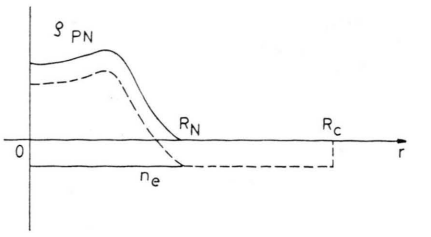

Fig. 1. Schematic charge distribution in the unit cell. ϱ_{PN} is the number density of protons in the nucleus as used in the Droplet-Model, n_e is the number density of the electrons. The dashed line is the resulting charge distribution. $R_N = 1.159\,A^{1/3}$ is the nucleus radius, $R_c = (3/4\,\pi\,\eta_N)^{1/3}$ is the cell radius, where n_N is the number density of nuclei.

We have ignored the cell-cell Coulomb interaction since this gives a small correction to the lattice energy. Then we get for the binding energy (including the lattice energy) the following modified mass formula

$$\begin{aligned} B(Z,A,R_c,R_N) = &\left(-a_1 + J\,\bar{\delta}^2 - \frac{1}{2}K\,\bar{\varepsilon}^2 + \frac{1}{2}M\,\bar{\delta}^4\right) + \left(a_2 + \frac{9}{4}\frac{J^2}{Q}\,\bar{\delta}^2\right)A^{2/3} \\ &+ (a_3 - \mu_3)A^{1/3} + C_1 Z^2 A^{-1/3}\left[1 - \frac{3}{2}\frac{R_N}{R_c} + \frac{1}{2}\left(\frac{R_N}{R_c}\right)^3\right] \\ &- C_2 Z^2 A^{-1/3}\alpha^2 - C_3 Z^2 A^{-1}\alpha - C^4 Z^{4/3} A^{-1/3}\left(1 + \frac{R_N}{R_c}\right) - C_5 Z^2 \alpha^2\,, \end{aligned} \tag{8}$$

where

$$\alpha \equiv \left[1 - \left(\frac{R_N}{R_c}\right)^3\right], \quad R_N = 1.1589\,A^{1/3}$$

$$\bar{\delta} \equiv \frac{I + 3\,C_1 Z^2 A^{-1/3}\alpha/16\,Q}{1 + 9\,J\,A^{-1/3}/4\,Q} \text{ (local asymmetry)} \qquad I \equiv (A - 2Z)/A\,, \tag{9}$$

and with

$$\bar{\varepsilon} \equiv [-2\,a_2 A^{-1/3} + L\,\bar{\delta}^2 + C_1 Z^2 A^{-4/3}\alpha]/K \tag{10}$$

denotes the deviation of the density from its nuclear matter value ϱ_0.

The values for the parameters are [26 b]

$a_1 =$	16.379 MeV	$M =$	5.0 MeV
$a_2 =$	22.76 MeV	$Q =$	21.63 MeV
$a_3 =$	9.34 MeV	$C_1 =$	0.745 MeV
$\mu_3 =$	12.54 MeV	$C_2 =$	1.47×10^{-4} MeV
$K =$	299.1 MeV	$C_3 =$	0.945 MeV
$L =$	120.6 MeV	$C_4 =$	0.569 MeV
$J =$	34.4 MeV	$C_5 =$	$C_1^2/64\,Q$.

In the following we discuss the results which we obtained for the density regime below ϱ_3 and compare them with preceeding calculations.

The properties of the outer crust ($\varrho < \varrho_2$) were first determined by Salpeter [5] who used the mass formula of Cameron [27] for the binding energy of the nuclei. Salpeter omitted the lattice energy and obtained the equilibrium nucleus present by a minimization procedure. Baym et al. [6] took into account the lattice energy and applied the semi empirical mass formula (LDM) of Myers and Swiatecki [26 a] with their shell correction term.

The near incompressibility and the strong symmetry energy of ordinary nuclei allow a fairly accurate description of the binding energy $E(Z,N)$ in terms of a LDM ("Liquid drop model"). To go beyond this stage of development requires that self-consistent calculations (Thomas-Fermi, Hartree-Fock) be performed. Alternatively the LDM can be extended by removing the constraint of incompressibility and allowing for a "neutron skin". An algebraic formulation for $B(Z,N)$, the "Droplet model" (DM), which introduces these two new degrees of freedom provides an opproximation to the more complex self-consistent calculations. In especial, the DM of Myers and Swiatecki [26] is the first order expansion of a microscopic model (Thomas-Fermi) for small values of $A^{1/3}$ and $(N-Z)/A$.

Table 2.1. Summary of the properties of neutron star matter below $\varrho_2 = 4.65 \times 10^{11}$ gr cm^{-3}, including shell corrections. The details of this analysis will be given elsewhere [28]. $\varrho_{\max}$ is the maximum mass-density at which the nuclei with charge Z and total baryon number A are present, p the corresponding pressure; μ_e is the electron chemical potential; T_m is the melting temperature calculated according to the formula $\Gamma_m K_B T_m \cong (z e)^2/R$ with $\Gamma_m = 80$ and cell-radius R (see Ref. [26]); Γ is the adiabatic index and $\varkappa = \left(n \frac{dp}{dn}\right)^{-1} \equiv \frac{1}{\Gamma \cdot p}$ the compressibility.

$\varrho_{\max}$ (g cm^{-3})	P (dyne cm^{-2})	Z	A	μ_e (MeV)	T_m (10^9 K)	Γ	$\varkappa$ (MeV^{-1} fm^3)
7.78×10^6	4.99×10^{23}	26	56	0.43	0.06	1.47	2.18×10^9
3.34×10^8	9.23×10^{25}	28	62	2.28	0.24	1.35	1.20×10^7
4.98×10^8	1.52×10^{26}	28	64	2.63	0.27	1.35	7.81×10^6
2.14×10^9	1.03×10^{27}	28	66	4.51	0.44	1.34	1.16×10^6
7.80×10^9	5.44×10^{27}	34	84	7.07	0.92	1.34	2.20×10^5
2.14×10^{10}	2.00×10^{28}	32	82	9.96	1.15	1.34	5.98×10^4
4.56×10^{10}	5.19×10^{28}	30	80	12.76	1.31	1.33	2.32×10^4
1.37×10^{11}	2.14×10^{29}	28	78	18.38	1.66	1.33	5.65×10^3
1.81×10^{11}	2.90×10^{29}	26	76	19.86	1.58	1.33	4.06×10^3
2.33×10^{11}	3.79×10^{29}	40	122	21.34	3.48	1.33	3.18×10^3
3.22×10^{11}	5.56×10^{29}	38	120	23.53	2.52	1.33	2.17×10^3
4.30×10^{11}	7.80×10^{29}	36	118	25.64	3.5	1.33	1.51×10^3
4.65×10^{11}	8.22×10^{29}	34	116	25.97	3.22	1.33	1.47×10^3

Using the DM to determine the binding energy of the nuclei adding their shell correction term we get (Koebke et al. [28]) the results for the outer crust which are given in Tab. (2.1). They differ from those of Salpeter [5] but show only slight modifications to the results of Baym et al. [6], e. g. our neutron-drip density is somewhat larger (ϱ_n-drip $= 4.65 \times 10^{11}$ g cm^{-3}). In the region above the neutron-drip density ϱ_2 Buchler and Barkat [7], applying a Thomas-Fermi calculation for the Wigner-Seitz cell, obtained substantially different results compared with earlier LDM calculations (Langer et al. [8]; Bethe et al. [9]).

They find that the charge number Z of the "clusters" ("nuclei") first increases from $Z = 29$ at $\varrho = 3 \times 10^{11}$ g cm^{-3} to a maximum of $Z = 35$ at $\varrho = 3 \times 10^{11}$ g cm^{-3} and then decreases until the clusters gradually evanesce just above $\varrho_3 \cong 10^{14}$ g cm^{-3}.

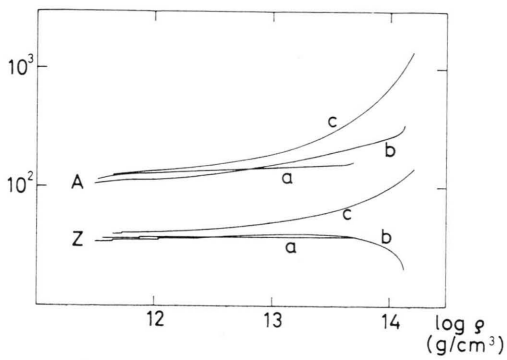

Fig. 2. Properties of nuclei in the crust beyond netron drip density.
a) Present calculation;
b) Calculation of Arponen [31];
c) Calculation of Baym et al. [10];
Z is the proton number, A the total baryon number of the nuclei.

In comparison Baym et al. [6] obtained $\varrho_3 = 2 \times 10^{14}$ g cm^{-3} and Z in excess of 100 (Figure 2).

Our results, which are based on the algebraic formula using the (DM) as given below together with two Thomas-Fermi treatments of the neutron gas are:

1. If we apply the calculations of Weiss and Cameron [24] with the modified interaction strength parameters as given below for the neutron gas we find the density $\varrho_3 = 4.9 \times 10^{13}$ g cm^{-3} at which the "nuclei" evaporate suddenly and then the matter would transform by a first order transition to a homogenous gas of neutrons, protons and electrons. At this density the maximum of $A = 162$ and $Z = 38$.

The use of the DM mass formula shows that there is no occurence of very massive nuclei in agreement with the results of Buchler et al. [11].

The jump $\Delta\varrho/\varrho$ of the matter density at the transition point would be $\cong 6\%$ and the transition ("evaporation") heat $\Delta f/f \cong 5.8\%$. A similar transition of first order can be extracted from the results presented by Langer et al. [8], by plotting carefully their values for equation of state, although they apparently overlooked this property.

To determine the transition at the boundary between the phase with nuclei (the crust) and the gas

phase, we used Eq. (4), which gives the chemical potential μ_1 for the first phase and μ_2 for the second phase, respectively, as a function of the pressure P. The two curves cross at the pressure $P_t = 4.43 \times 10^{31}$ dyne/cm^2 which correspond to $\varrho_3 = 4.9 \times 10^{13}$ g cm^{-3}.

2. Otherwise applying the Thomas-Fermi calculations given by Myers and Swiatecki [26] for the neutron gas we find that the possible phase transition mentioned above is at least shifted to higher densities or, probably does not occur at all. To give a consistent picture of the phase transition at high density, ($\varrho \gtrsim 10^{14}$ g cm^{-3}) the DM dependence of the outside gas must the found [29].

2.2. *The Quantum Fluid Regime*

In nuclear physics the energy per particle E/N is conveniently expressed by means of the Fermi-wave number k_F (fm^{-1}) which is related to the particle density $n = 3\pi^2 k_F^3$. In the low-density gas approach the interaction energy is expanded in a series of k_F, the kinetic energy (E_{kin}/N) being $(E_{kin}/N) = a k_F^2$ (MeV) with $a = 12.2$ (MeV fm^{-2}). The lowest-order contributions to the potential energy are $E_{pot}/N = b k^3{}_F + c k^5{}_F \ldots$ the coefficients being independent of k_F. In principle it would therefore suffice to know E/N over a comparatively small density interval to high accuracy to determine the various coefficients. These would allow then to extrapolate E/N to high densities. For all cases studied we find that E/N can indeed be fitted over the whole density range of interest by

$$W = E/N = a k_F^2 + b k_F^3 + c k_F^5$$

however it is sometimes convenient to consider (a) as a free parameter to include possible eletron-proton contributions or to allow for a $k^7{}_F$-term to describe the very high density regime. In the low density regime where a Coulomb-lattice is present analytic fits are more involved and given in Appendix A. As pointed out above different approaches have been used to derive expressions for the parameters a, b and c. Erkelenz, Hohlinde and Alzetta [30] tried to derive a more fundamental expression for the nucleon-nucleon interaction potential by means of one boson exchange forces and applied lowest order Brueckner-theory. Their potential has many attractive features as 1) it is based on known boson masses and estimated or measured coupling strengths

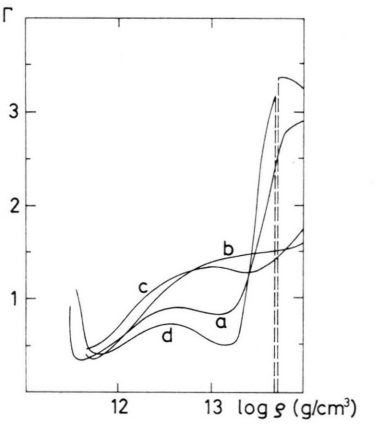

Fig. 3. The adiabatic index Γ as a function of density ϱ in the crust regime for several equations of state.
a) Langer et al. [8]; b) Baym et al. [10]; c) Arponen (EOS 3); d) present work (EOS 1). We have denoted by the dashed lines the region of phase transition where the pressure is constant ($\Gamma \to 0$).

Table 2.2. Properties of neutron star matter beyond neutron drip density. X: percentage of charged particles, μ_n: chemical potential of neutrons, $T_{c,n}$: critical temperature of $^1S_0$ neutron-superfluidity, $H_{c,15}$: critical magnetic field in units 10^{15} Gauss, $T_{c,p}$: critical temperature for proton $^1S_0$ superconductivity, the other notations are the same as in Table 2.1 a. The critical quantities of $^1S_0$ pairing are from [22].

ϱ (g cm^{-3})	p (MeV·fm^{-3})	z	A	μ_e (MeV)	μ_n (MeV)	T_m (10^9 K)	X	$T_{c,n}$ (10^9 K)	$T_{c,p}$ (10^9 K)	$H_{c,15}$
4.68×10^{11}	5.2×10^{-4}	37	126	25.8	0.04	3.8	28.6	2.6	—	—
1.20×10^{12}	8.2×10^{-4}	38	133	27.2	0.71	4.3	15.2	6	—	—
4.89×10^{12}	2.6×10^{-3}	38	147	32.8	1.81	4.9	5.5	9	—	—
1.06×10^{13}	5.4×10^{-3}	38	156	38.0	2.45	5.3	3.2	7	—	—
2.31×10^{13}	1.0×10^{-2}	38	165	44.7	2.97	5.6	1.7	6	—	—
5.01×10^{13}	3.3×10^{-2}	38	182	56.2	3.95	6.2	1.1	4	—	—
7.39×10^{13}	9.4×10^{-2}	38	228	64.6	5.60	7.3	1.2	3.2	—	—
8.41×10^{13}	1.3×10^{-1}	43	327	67.6	6.47	9.7	1.3	2.6	—	—
9.58×10^{13}	2.1×10^{-1}	?	?	72.4	7.89	?	1.5	2.2	2.6	1.8
1.18×10^{14}	4.1×10^{-1}	—	—	79.4	11.0	—	2.1	2.0	3	2.0
3.01×10^{14}	7.0	—	—	128.	61.6	—	8.0	?	5	4.9

only, 2) it gives a satisfactory binding energy and saturation density, 3) it incorporates relativistic features and off-shell behaviour which are inacessible to experiment but needed in nuclear-matter and neutron-star-matter calculations. The neutron-matter properties of this momentum space OBEP have been calculated to the first order Brueckner-Goldstone reaction matrix G using the angle averaged Pauli operator, the effective mass approximation for the hole spectrum to be determined self-consistently and a free particle spectrum.

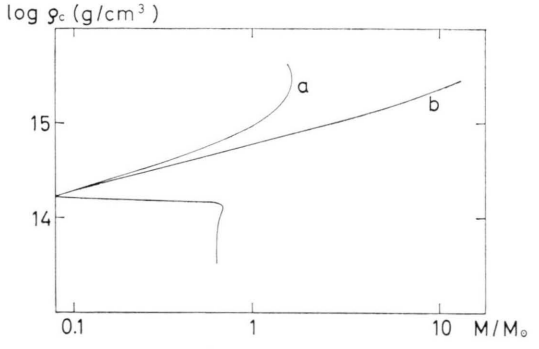

Fig. 4. General relativstic and Newtonian neutron star models for EOS 3. ϱ_c ist the central density, $M/M_\odot$ the gravitating mass in units of the mass of the sun.
a) general relativistic models; b) Newtonian models.

The details of their calculations are summarized in [30]. Similar calculations as discussed above have also been performed by Arponen [31]. Both equations of state [30, 31] have been fitted analytically as a function of the particle number density and are given in the Appendix A. More recently Källman has used the theory of Fermi liquids [32] where polarization effects of the matter are included. Surprisingly he finds [32] that this increases the pressure for a given density roughly by a factor 2. While the overall features of neutron stars are hardly affected by this refinement it does have an interesting effect on neutron star binding as we shall show below in the third section (EOS 3 b and neutron star sequence 3 b).

2.3. The Limiting Form of the Equation of State

Beyond $k_f \cong 2\,(\mathrm{fm}^{-1})$ the reliability of nuclear many-body techniques is difficult to estimate since the three-body and higher order correlations become increasingly important. If at these densities the hard-core interaction is still a valid description for the two-body interaction one might try instead to expand the energy per particle about a formally divergent state of energy, namely about that density where the particles hard-cores touch each other. Such an approach would therefore provide the opposite limit from the gas-parameter expansions, making possible an interpolation to intermediate densities. Such a tentative approach has been taken by Cole [30] some years ago. Briefly his procedure can be described as follows.

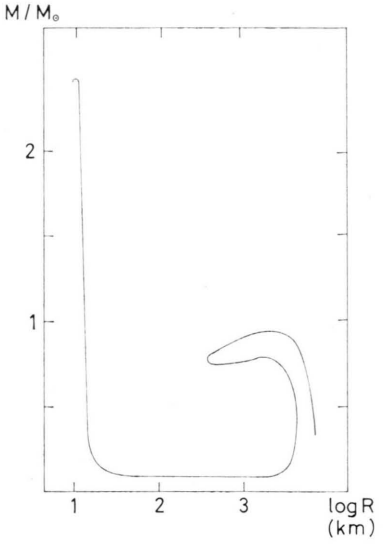

Fig. 5. Total mass M as a function of the radius R for EOS 1. Passing the curve from the right (so increasing the central density ϱ_c), all star models remain stable until the first maximum of about 1.1 $M_\odot$ is reached (stable white dwarfs $\varrho_c \lesssim 7 \times 10^9\,\mathrm{gr/cm^3}$). They become unstable down to the next minimum of 0.73 $M_\odot$ ($\varrho_c \cong 5 \times 10^{13}\,\mathrm{gr/cm^3}$). Again there is a stable area up to $M = 0.76\,M_\odot$ ($\varrho_c \cong 9 \times 10^{13}\,\mathrm{gr/cm^3}$) and then unstability down to $0.1\,M_\odot$ ($\varrho_c \cong 1.2 \times 10^{14}\,\mathrm{gr/cm^3}$. Then follow stable neutron stars up to the next maximum of 2.41 $M_\odot$ ($\varrho_c \cong 2 \times 10^{15}\,\mathrm{gr/cm^3}$).

For a one-dimensional system of hard spheres of radius a in a length L the energy per particle is known exactly. The ground state corresponds to $W = \mathrm{A}\,(\hbar^2/2\,m)\,(1/n - 1/n_0)^{-2}$ where $n \equiv N/L$ is the density in one dimension, $n_0 = a^{-1}$ and $A = \pi^2$. In three dimensions one finds by analogy $W = A\,(\hbar^2/2\,m)\,(n^{-1/3} - n_0{}^{-1/3})^{-2}$ where $n_0 = a^{-3}$ and $A \cong \pi^2$. While this model is not realistic for realistic nuclear forces, Cole notes that it may have some of the qualitative features of the actual close packed system. Two points should be stressed: a) the result for W is independent of particle statistics, therefore such a model would ignore possible differences for hyperons as far as statistics are concerned and b) the particles are localized in a lattice and therefore distinguishable. That neutronic matter might

indeed form a quantum lattice has recently been suggested by various authors [23]. However so far we have included in W only the repulsive part of the interaction and neglected the attractive part of the nuclear force which binds the system into a lattice.

For a system of interacting point particles this would lead [34] to a contribution proportional to the particle number density or more generally to a power of the energy density [35] so we probably overestimate the attractive part of hard-spheres if we add to W a negative term $-Bn$. If such a fit is at least qualitatively correct it should join smoothly to the low density expansions for intermediate densities. It turns out that for the reasonable value of the hard-core radius $a = 1/2$ Fermi such a fit is indeed possible. We used the numerical results of Arponen [31] for the intermediate region $0.09 \leqq n \leqq 0.322$ and got $A = 0.684$.

The properties of this equation of state (EOS 4) are also given in the Appendix A.

The main motivation in such a strong extrapolation and manifestly non-Lorentzian procedure lies of course in the interest to see how strongly actual neutron star model parameters, especially their mass, are affected. The results are discussed in detail in Sec. 3, here we remark only that the high density mass limit is not affected seriously.

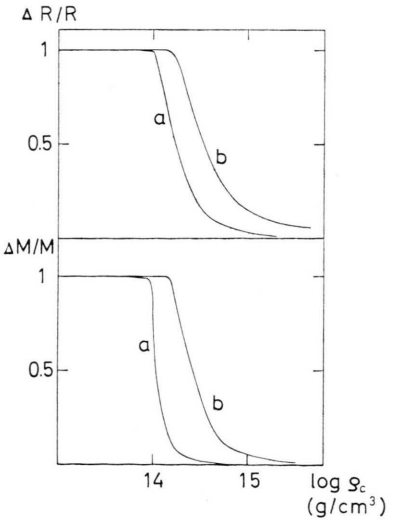

Fig. 6. Contribution of the crust to the total mass and the radius of neutron stars for EOS 1 (a) and EOS 3 (b).

In a quite similar spirit, namely to explore the consequences of various assumptions about internucleon forces, Pandharipande [36] has considered different models for hyperonic equations of state. Here we used Pandharipande's equation of state A which has a phase transition at $P = 1.17$ MeV fm^{-3} and n jumps from 0.13 to 0.842 fm^{-3}. The properties of this equation of state (EOS 5) are summarized in the Appendix A. His results are comparable though not quite as drastic as those by Libby and Thomas [37] presented some years ago and should of course be considered with reserve but they point towards a conceptually interesting possibility of a third family of stars (Heintzmann, Hillebrandt [38]) namely pure hyperon stars. Pandharipande finds for two specific sequences of hyperon matter that the energy per particle decreases as the density increases in a certain density interval. He argues that such a behaviour reveals in reality a phase transition between a neutronic and hyperonic state. It should be emphasized that it is not unconceivable that a more accurate treatment could lead even to a bound state indicating therefore a

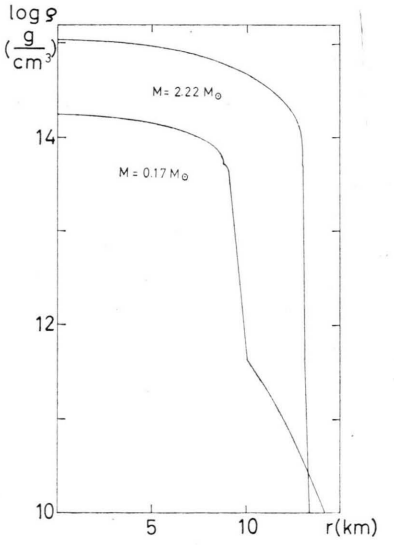

Fig. 7. Density distribution of two neutron star models resulting from EOS 1.

third state of matter in stars. While such matter would be extremely unstable in the laboratory-ordinary nuclear matter is more tightly bound by many MeV per particle – it could be stablized by the strong gravitational attraction if enough particles are lumped together as will be seen in Sec. 3 below:

Concluding this section we remark that we have been unable to give a unique, convincing treatment of the neutron star matter problem but we feel that

the final answer – if there will ever be a satisfactory theory – will lie somewhere between the extremes considered above. Moreover one should also keep in mind that besides the known nuclear forces possible weak interactions which are stronger than gravitational forces, but so weak that they have escaped experimental detection can alter considerably the above considerations (Heintzmann [39]).

3. Neutron Star Models

3.1. Theory of Gravitation

Before we come to calculate and discuss the properties of neutron star models which result from the equation of state presented in the previous section, a few words on theories of gravity are in order. As we have seen before a strong extrapolation from everyday physics was necessary to derive the properties of superdense matter. However the basic principles and methods are unquestioned (Schrödinger equation) and well in touch with experiments (nuclear forces and many-body techniques).

Unfortunately the same cannot be said about the theory of gravitation which would adequately describe the macroscopic structure of objects with superdense matter. On dimensional grounds we expect any relativistic theory of gravitation to deviate essentially from Newtonian i. e. non relativistic gravity as soon as $R_s = G M/c^2$ approaches the dimensions of the system (G gravitational constant). In the solar system R_s/R is of the order $\sim 4 \times 10^{-6}$ and even in white dwarfs it is only $\sim 10^{-2}$. Therefore if we were only interested in ordinary stars or white dwarfs careful measurements of gravitational effects (light-bending, time-delay, gyroscope-precession etc.) in the solar system would probably soon determine the post-Newtonian version of gravity to sufficient accuracy for the description of these latter objects and such a program is indeed under way. However, both for neutron stars and for the early universe the relativistic theory is needed in its full glory and not only to its post Newtonian order. It is therefore to be kept in mind that everything we derive below is really a consequence of Einsteins theory of gravitation or one of its rivals the Jordan-Brans-Dicke theory. As far as we are aware of neutron star models have not been explored in other rival theories but we predict that especially for the so called linearized theories large differences are to be expected from the results presented below.

In Einsteins theory the equation for the hydrostatic equilibrium is given (in Schwarzschild coordinates) by

$$\begin{aligned} \mathrm{d}m/\mathrm{d}r &= 4\pi r^2 \varrho\,, \\ -\mathrm{d}P/\mathrm{d}r &= G\,\frac{(\varrho + P/c^2)\,(m + 4\pi r^3 P/c^2)}{r^2(1 - G\,m/r\,c^2)}\,, \end{aligned} \tag{11}$$

and its Newtonian limit by

$$\begin{aligned} \mathrm{d}m/\mathrm{d}r &= 4\pi r^2 \varrho\,, \\ -\mathrm{d}P/\mathrm{d}r &= G\,\varrho\, m/r^2\,. \end{aligned} \tag{12}$$

In Eq. (11) $m(r)$ is the gravitating mass inside a sphere of surface area $4\pi r^2$ and ϱ the total mass energy density:

$$\varrho = m_n n + \varepsilon/c^2\,.$$

The main difference between both Eqs. (11) and (12) is that in the general relativistic case the sphere of surface area $4\pi r^2$ and ϱ the total mass and the total mass density.

In J-B-D-theory [40] we have the following set of equations in Schwarzschild coordinates, φ being the additional scalar potential:

$$\frac{\mathrm{d}M(r)}{\mathrm{d}r} = 4\pi r^2 \left[\frac{\varrho}{\varphi} + \frac{\omega\,\varphi'^2}{16\pi\varphi}\,\frac{c^2}{G}\,\frac{r-2m}{r}\right] + \frac{1}{\varphi}\left[\frac{(3P/c^2 - \varrho)}{3+2\omega}\right] r^2 \tag{13 a}$$

$$-\frac{\mathrm{d}P(r)}{\mathrm{d}r} = G\,\frac{P/c^2 + \varrho}{r(r-2m)}\left[M + 4\pi r^3\left(\frac{P}{\varphi c^2} - \frac{\omega}{4\varphi^2}\,\frac{c^2}{G}\left(1 - \frac{2m}{r}\right)\varphi'^2\right)\right] \tag{13 b}$$

$$\varphi'' + \left[\frac{3}{r} - \frac{r-2m}{r^2} + \frac{4\pi G}{\varphi c^2}\,(3P/c^2 - \varrho) - \frac{\omega\,\varphi'^2}{2\varphi^2}\,(r-2m) - \frac{8\pi G}{\varphi c^2}\,\frac{r(3P/c^2 - \varrho)}{(3+2\omega)}\right]\varphi' = \frac{8\pi G}{(3+2\omega)c^2}\,(3P/c^2 - \varrho)\,\frac{r}{(r-2m)} \tag{13 c}$$

with

$$m = m(r) = G\,M(r)/c^2 \tag{13 d}$$

and

$$\varphi'(0) = 0\,, \quad \varphi(\infty) = 1\,, \quad m(0) = 0\,, \quad P(0) = P_c\,, \quad P(R) = 0\,. \tag{13 e}$$

The integration procedure [40, 41] is somewhat more involved than in the Einsteinian case due to the presence of a scalar gravitational field which is coupled to the trace of the energy momentum tensor. The numerical results are shown in Figure 8.

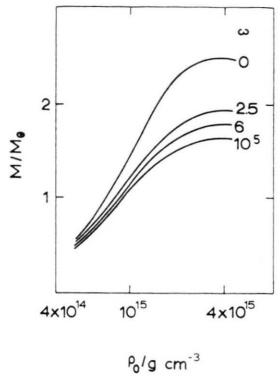

Fig. 8. Mass-density relationship for various values of the J−B−D coupling constant ω for Arponen's [31] equation of state, ϱ_0 the central density; $M/M_\odot$ the mass in units of the mass of the sun.

3.2. Nonrotating Neutron Star Models

In Newtonian theory the gravitational energy of a spherical body is proportional to $G M^2/R$, where M is the total mass and R is the radius of the sphere, while the internal energy for an equation of state of form $P = P_0(\varrho/\varrho_0)^\Gamma$ with constant Γ is proportional to $M^\Gamma/R^{3(\Gamma-1)}$ [42]. If the sum of both has an extremum, this extremum is a maximum only if $\Gamma < 4/3$. Since for all equations of state presented in this paper Γ exceeds 4/3 in the high density region, there is no upper mass limit in Newtonian theory for neutron stars.

The differences between Newtonian and general relativistic neutron star models are shown in Fig. 4 for the equation of state of Arponen (EOS 3). It is seen that differences become important only for central densities beyond nuclear matter density.

From the static, non-rotating models the mean properties of general relativistic neutron stars can be derived. The results are listed in Tables 3.1 – 3.5 for our equations of state EOS 1 – EOS 5. The models are different not only for high densities, as would be expected from the discussion in chapter 2, but also in the low-density region. The minimum mass of a stable, bound neutron star differs by about a factor of two. However, for the two equations of state EOS 1 and EOS 3 which take into account protons, electrons and nuclei the difference

Table 3.1. Star sequence for EOS 1. ϱ_c is the central density, M the gravitating mass in units $M_\odot$ of the sun's mass, R the radius, E_b the binding energy per baryon, I the general relativistic moment of inertia. [a] unstable stars.

ϱ_c (g cm^{-3})	M ($M_\odot$)	R (km)	$E_{bind/N}$ (MeV)	I (10^{44} g cm^2)
1.66×10^6	0.40	9898	− 2.31	1.46×10^6
8.46×10^7	0.92	4068	− 2.42	4.60×10^5
5.00×10^8	1.03	2763	− 2.46	2.05×10^5
[a] 2.58×10^9	1.00	1857	− 2.44	7.34×10^4
[a] 1.30×10^{10}	0.94	1199	− 2.39	2.34×10^4
[a] 6.51×10^{10}	0.86	745.9	− 2.28	7.08×10^3
[a] 3.26×10^{11}	0.79	450.9	− 2.09	2.09×10^3
[a] 1.64×10^{12}	0.75	407.3	− 1.97	1.53×10^3
8.19×10^{12}	0.74	427.8	− 1.93	1.63×10^3
4.10×10^{13}	0.75	430.7	− 1.95	1.69×10^3
7.56×10^{13}	0.75	632.8	− 1.98	3.67×10^3
1.43×10^{14}	0.11	25.31	− 1.65	0.583
1.69×10^{14}	0.17	17.75	− 5.52	0.993
2.55×10^{14}	0.42	14.23	−20.8	3.42
4.37×10^{14}	1.05	14.14	−56.3	13.0
7.44×10^{14}	1.83	13.97	−101	26.7
1.11×10^{15}	2.23	13.32	−127	32.9
2.07×10^{15}	2.41	11.92	−138	30.2
[a] 2.27×10^{15}	2.41	11.71	−137	28.8

Table 3.2. Neutron star models from EOS 2 (E.H.A.). [b] unbound neutron stars. The other notations are the same as in Table 3.1.

ϱ_c (g cm^{-3})	M ($M_\odot$)	R (km)	$E_{bind/N}$ (MeV)	I (10^{44} g cm^2)
[b] 6.77×10^{13}	0.15	82.63	2.39	2.29
[b] 1.02×10^{14}	0.19	37.93	0.68	2.17
1.36×10^{14}	0.23	28.15	− 1.16	2.39
3.83×10^{14}	0.52	15.80	−17.5	4.08
5.29×10^{14}	0.73	15.08	−30.0	5.15
8.19×10^{14}	1.13	13.31	−56.8	8.62
1.03×10^{15}	1.37	12.65	−74.8	12.9
2.02×10^{15}	1.93	10.88	−124	18.3
3.03×10^{15}	2.01	9.93	−135	17.5

Table 3.3 a. Neutron star models from EOS 3 a (Arponen). Notations as in 3.1 and 3.2.

ϱ_c (g cm^{-3})	M ($M_\odot$)	R (km)	$E_{bind/N}$ (MeV)	I (10^{44} g cm^2)
[a] 3.37×10^{13}	0.65	808.9	− 1.64	4.37×10^3
6.74×10^{13}	0.65	9.55.8	− 1.65	6.35×10^3
1.35×10^{14}	0.69	1687	− 1.72	2.66×10^4
[b] 1.69×10^{14}	0.09	650.7	3.28	26.7
2.38×10^{14}	0.14	22.46	− 0.32	0.503
3.06×10^{14}	0.21	15.24	− 6.23	1.04
5.18×10^{14}	0.50	12.09	−35.2	3.34
7.01×10^{14}	0.76	11.67	−46.9	5.69
1.01×10^{15}	1.11	11.31	−72.8	8.93
1.41×10^{15}	1.38	10.88	−102	11.4
2.00×10^{15}	1.55	10.32	−111	12.4
2.97×10^{15}	1.63	9.67	−124	12.0
[a] 3.43×10^{15} [9]	1.63	9.46	−124	11.5

Table 3.3 b. Neutron star models from EOS 3 b (Källman). Notations as in 3.1 and 3.2.

ϱ_c (g cm^{-3})	M ($M_\odot$)	R (km)	$E_{bind/N}$ (MeV)	I (10^{44} g cm^2)
b 8.46×10^{13}	0.15	51.14	2.54	1.84
1.70×10^{14}	0.27	22.65	− 4.74	2.67
3.43×10^{14}	0.48	16.27	−19.9	4.45
5.21×10^{14}	0.69	14.41	−35.2	6.25
8.02×10^{14}	0.99	13.06	−57.3	8.85
1.21×10^{15}	1.32	11.97	−83.2	11.6
1.80×10^{15}	1.59	10.95	−107	13.5
2.35×10^{15}	1.72	10.27	−120	13.8
2.98×10^{15}	1.78	9.66	−124	13.5

Table 3.4. Star models for the Cole hard-sphere equation of state. Notations as in 3.1.

ϱ_c (g cm^{-3})	M ($M_\odot$)	R (km)	$E_{bind/N}$ (MeV)	I (10^{44} g cm^2)
8.96×10^{14}	1.13	11.46	− 73.4	11.1
1.10×10^{15}	1.47	11.28	− 99.8	17.0
1.33×10^{15}	1.78	11.06	−126	22.5
1.59×10^{15}	2.03	10.77	−150	26.7
2.27×10^{15}	2.30	10.04	−182	29.2
2.75×10^{15}	2.33	9.65	−187	29.6
a 3.41×10^{15}	2.32	9.28	−186	28.4

Table 3.5 a and 3.5 b. Models of hyperon stars for EOS 5 (Pandharipande). *Upper* table: hyperon stars with phase transition. *Lower* table: pure hyperon stars with $\varrho_s = 1.54\times10^{15}$ and $p(\varrho_s)=0$. Notations as in 3.1.

ϱ_c (g cm^{-3})	M ($M_\odot$)	R (km)	$E_{bind/N}$ (MeV)	I (10^{44} g cm^2)
1.71×10^{15}	0.13	80.17	− 0.15	0.837
2.06×10^{15}	0.19	8.28	− 17.2	0.229
2.43×10^{15}	0.38	6.50	− 45.9	0.587
3.44×10^{15}	0.84	5.95	−115	3.40
5.40×10^{15}	1.19	5.89	−168	6.07
8.21×10^{15}	1.26	5.57	−180	6.23
a 9.65×10^{15}	1.26	5.44	−178	5.98
1.89×10^{15}	0.07	2.68	− 0.42	0.066
2.06×10^{15}	0.14	3.36	− 15.2	0.216
2.43×10^{15}	0.29	4.15	− 39.9	0.689
3.44×10^{15}	0.88	5.54	−127	4.22
5.40×10^{15}	1.26	5.72	−189	7.30
8.21×10^{15}	1.32	5.46	−202	7.34
a 9.65×10^{15}	1.32	5.35	−200	7.04

is only 20% and it is to be expected that inclusion of these effects into EOS 2 which is for pure neutron matter will lower the minimum mass. It seems therefore that $0.10\,M$ is a lower mass limit for bound stable neutron stars. The reason that there is still uncertainty about this limit which lies entirely within regime where nuclear many-body techniques apply and can be trusted is seen from Equation (12). To construct star models not only ε as a function of (n) is needed but also its second derivative. But as the compressibility cannot even be measured for nuclear matter the determination of $\varkappa$ is a difficult (and sometimes controversial) question in nuclear physics.

The differences for the maximum stable mass of our neutron star models are also not very large and apparently comparable to the minimum mass uncertaintly discussed above. EOS 1 seems to be an upper limit in stiffness to any 'reasonable' equation of state [38] since the hard sphere EOS 4 of Cole gives similar results and so does an incompressible fluid. Moreover we found that an additional term to in EOS 4 $\Delta\varepsilon = -B\,n^2$ as discussed in section 2 would lower the energy for small densities and give a stiffer equation of state and therefore lead essentially to the same mass limit. However as mentioned before reservations have to be made concerning forces at high densities and it could therefore well be that the actual mass limit is lower than those derived here. To conclude this section we discuss the possibility of another class of stars with densities far beyond neutron star density. Such hyperon star models result e. g. from Pandharipande's equation of state A [36] (here referred to as EOS 5). We follow Pandharipande's interpretation and set $P = \text{constant} = 1.17$ MeV fm^{-3} for $1.4\times10^{15}\,\text{g cm}^3 \leqq \varrho \leqq 2\times10^{14}\,\text{g cm}^3$, and below 2×10^{14} g cm^3 we use EOS 3. The star models then have a core of hyperonic matter, including nearly all of their mass, and a thin outer layer, its thickness decreasing from about 300 m to 70 m if the central density increases from 2×10^{15} g cm^3 to 9×10^{15} g cm^3. The maximum stable mass of such objects is somewhat smaller than of ordinary neutron stars, while the minimum stable mass is the same for both. We want to point out that for hyperon stars the binding energy per particle is larger than for neutron stars with the same total particle number (see Table 3.5). There is further no problem with the standard criterium that the velocity of sound $v_s = (\mathrm{d}P/\mathrm{d}\varrho)^{1/2}$ be smaller than C, the velocity of light. So if the equation of state for hyperonic matter is of the type calculated by Pandharipande, there is indeed a possibility for a third family of stars, namely hyperon stars.

3.3. Rotation

Another important parameter of a neutron star is his moment of inertia which in Newtonian theory for a rigid rotating spherical body is

$$I_{\text{Newton}} = (8\pi/3)\int_0^R \varrho\, r^4\, \mathrm{d}r\,. \tag{18}$$

In Einstein's theory one gets for slowly rotating spherical objects an additional equation to the TOV-equation describing the dragging of inertial frames along the rotational axis [43]. Setting $\bar{\omega} = \omega - \Omega$ where Ω is the angular velocity of the star as measured by a distand observer and ω is the angular velocity of the inertial frames along the rotational axis, this equation is

$$\left((1 - 2Gm/rc^2)^{1/2}\, e^{-\nu/2}\, r^4\, \bar{\omega}'\right)' = \frac{16\pi G r^4}{c^2}\,\frac{e^{-\nu/2}}{(1-2Gm/rc^2)^{1/2}}\,(\varrho + P/c^2)\,\bar{\omega} \tag{19}$$

where

$$e^{\nu/2} = \left\{\exp \int_0^{P=P(r)} \mathrm{d}P/(P+\varrho c^2)\right\}(1-2Gm/rc^2)^{1/2}\,. \tag{20}$$

Equation (19) has to be solved numerically with boundary conditions $\bar{\omega}(\infty) = \Omega' \sim A\, r (r \to 0)$.

A can be determined by studying the asymptotic behaviour of e^{ν} and $e^{-\lambda}$ as $r \to 0$ and imposing that $\bar{\omega}$ remains finite.

After having determined $\bar{\omega}(r)$ the moment of inertia can be calculated either by

$$I = I_{\text{Einstein}} = \frac{8\pi}{3}\int_0^R \mathrm{d}r\,\frac{r^4(\varrho + P/c^2)}{(1-2Gm/rc^2)^{1/2}}\,\frac{\bar{\omega}}{\Omega}\,e^{-\nu/2} \tag{21}$$

or [by substituting (19) into (21)] by

$$I = \frac{c^2}{6G}\,\frac{R^4\,\bar{\omega}'}{\Omega}\bigg|_{r=R}\,. \tag{22}$$

The general relativistic effect on the moment of inertia becomes important for very massive stars and we found numerically $I \cong I_{\text{Newton}}$ near the limiting mass for all equations of state (see Table 3.6). In Tables 3.1 – 3.5 I is listed. Near the maximum stable mass I decreases if M increases, so that the neutron star will speed up if a mass ΔM is added but this is not a general relativistic effect, cf. Table 3.6.

To finish the discussion of slowly rotating neutron stars we make some short remarks whether our assumption of "slow rotation" is a good approximation and how the other properties as for example the mass-quadrupole moment behave for realistic pulsars.

The "critical angular velocity" is reached if the rotating star begins to shed mass at its equator because of the contrifugal forces and is given by

$$\Omega c = (GM/R^3)^{1/2}\,. \tag{23}$$

For our neutron star models Ω_c is between $4\times10^2\,\mathrm{sec}^{-1}$ for the smallest bound stars and $2\times10^4\,\mathrm{sec}^{-1}$ for the most massive stars. For stars with moments of inertia large enough to explain the energy output of the crab nebula Ω_c is of order $2\times10^3\,\mathrm{sec}^{-1}$, therefore $\Omega\,\mathrm{crab}/\Omega c \leqq 0.1$ so that even the fastest known pulsar is a nonrelativistically rotating object.

Since the mass-quadrupole moment is proportional to $(\Omega/\Omega_c)^2$ this quantity is small for observed pulsars unless there is some strain frozen-in from an epoch where they rotated faster and this effect will be discussed in Section 4.

ϱ_c (g cm^{-3})	I_{GR}/I_N EOS 1	EOS 3
2.55×10^{14}	1.06	1.03
3.44×10^{14}	1.10	1.05
5.20×10^{14}	1.19	1.09
8.85×10^{14}	1.34	1.18
1.10×10^{15}	1.43	1.23
1.53×10^{15}	1.55	1.32
2.00×10^{15}	1.58	1.40
2.40×10^{15}	—	1.45
3.12×10^{15}	—	1.51

Table 3.6. Ratio of general relativistic (GR) and Newtonian (N) moment of inertia. ϱ_c is the central mass density.

4. Theories Related to Observation

4.1. Pulsar Glitches and Timing Residuals

After more than three years of continued observation of the Crab and Vela pulsar and of some 20 further pulsars the following picture has evolved [44]:

1) The faster (Crab) pulsar shows more frequent ($\cong$ 2/year) but smaller ($\Delta\Omega/\Omega \cong 10^{-8}$) speedups than the slower and therefore probably older (Vela) pulsar ($\cong$ 0.5/year, $\Delta\Omega/\Omega \cong 2\times10^{-6}$).
2) Timing residuals which can be interpreted as "noise" are roughly a factor 10 larger for the Vela [44] than for the Crab pulsar.
3) No speedup or noise of comparable size has been observed any of the slower pulsars which are also monitored regularly.

Ruderman and others [45] have given a simple and in many respects satisfactory explanation of these speedups by the two-component neutron star model. Their final answer is that the smaller speedups are related to different types of neutron stars than the big ones

in that the smaller ones (of the Crab) are due to crustquakes whereas the Vela speedups are due to ("small") quakes of a rather brittle core. It has been shown elsewhere [47] that for the big glitches the core would have to solidify at a large angular velocity $\gtrsim 2\times 10^3\,\mathrm{sec}^{-1}$.

In addition to the above mentioned facts 1) – 3) pulsars show a peculiar "healing" behaviour after a speedup. Specifically after a glitch of order $\Delta\Omega/\Omega$ the change in $\Delta\dot{\Omega}/\dot{\Omega}$ is much larger than $\Delta\Omega/\Omega$ and this is explained [44] if one assumes that in a considerable part of the star both neutrons and protons are superfluid (see Table 2.2).

In this model the speed-ups are related to sudden changes ΔI in the moment of inertia of the neutron star, during which angular momentum is conserved:

$$0=\Delta(I\cdot\Omega)=I\,\Delta\Omega+\Omega\,\Delta I\,. \tag{23}$$

The changes in I are due to a cracking of a solid component of the neutron star which for the smaller speed-ups of the Crab pulsar is assumed to be the star's crust and for the larger ones an inner neutronic quantum crystal. In the two-component model of a normal, charged and a superfluid neutral component (indices c and n) a phenomenological description [44] gives for the observed jump discontinuities:

$$\frac{\Delta\dot{\Omega}}{\dot{\Omega}}=\frac{\Delta\Omega}{\Omega}\,\frac{T}{\tau}\left(1-\frac{\Delta I_n/I_n}{\Delta I_c/I_c}\right) \tag{24}$$

$$Q\equiv\frac{(\Delta\dot{\Omega})^2}{\Delta\Omega\,\Delta\ddot{\Omega}}=\left(1-\frac{\Delta I_n/I_n}{\Delta I_c/I_c}\right)\frac{I_n}{I_n+I_c} \tag{25}$$

where $T\equiv-\Omega/\dot{\Omega}$ is the slow-down time and τ the healing time. Since the slow-down time T is much larger than the healing time a natural explanation is provided for $\Delta\dot{\Omega}/\dot{\Omega}\gg\Delta\Omega/\Omega$ and $\Delta\Omega/\Omega$ is related to a macroscopic coupling time [48] between superfluid neutrons and charged particles:

$$\tau\approx 0.7\cdot 10^3\,\frac{\Omega_{c,2}}{\Omega}\,\frac{T_e^{\,2}}{T_n\,T}\,\frac{\hbar}{\Delta_n}\cdot\left(\frac{k\,T_n}{2\,m_n\,c^2}\right)^{1/2}\exp\left(\frac{\pi}{4}\,\frac{\Delta_n^{\,2}}{k^2\,T_n\,T}\right), \tag{26}$$

where Ω is the angular frequency, $\Omega_{c,2}=\pi^2\,\Delta_n^{\,2}/4\,\hbar\,k\,T_n$ is the upper critical angular frequency, $T_i=$ Fermi temperature of component i, $k=$ Boltzmann's constant, and $\Delta_n=$ suprafluid gap energy.

We present in Table 4.1 Q and $\Delta I/I$ for EOS 1. For details of the model the reader is referred to [47].

Table 4.1. Pulsar-speed-up parameters for EOS 1. ϱ_0 central mass density, I total moment of inertia, I_c moment of inertio of the charged component (the core in our calculations), $\Delta I_c/I_c$ relative change in the moment of inertia of the charged component through monopole and quadrupole deformations, $Q=(\Delta\dot{\Omega})^2/\Delta\Omega\,\Delta\ddot{\Omega}$. The solidification density has been chosen as $7.3\times 10^{14}\,\mathrm{g\,cm}^{-3}$. The solidification angular velocity is $\Omega_s=300\,\mathrm{sec}^{-1}$, the glitch angular velocity $\Omega_g=30\,\mathrm{sec}^{-1}$. All $\Delta I_c/I_c$ scale as (Ω_s).

ϱ_0 ($10^{15}\,\mathrm{g\,cm}^{-3}$)	I ($10^{44}\,\mathrm{g\,cm}^2$)	I_c ($10^{44}\,\mathrm{g\,cm}^2$)	$10^3\,\Delta I_c/I_c$	Q
0.86	21.2	0.42	0.61	0.61
0.98	21.7	1.45	0.63	0.38
1.11	21.7	2.70	0.45	0.25
1.24	21.3	3.92	0.39	0.17
1.54	19.9	5.77	0.31	0.08

4.2. *Quadrupole Moments of Neutron Stars*

We conclude our discussion of the rotational properties of neutron stars with a treatment of the quadrupole deformations. We shall give here only a simplified Newtonian treatment and the reader is referred to [43] or Thorne [49] for the corresponding Einsteinian analysis. Small deviations from sphericity are necessary to impede a magnetic field alignment with the axis of rotation [50] and large deviations could lead to triaxial configurations (Jacobian ellipsoids) which would give rise to the emission of gravitational waves [51].

In Newtonian theory the quradrupole moments $Q_{\alpha\beta}$ are related to the moments of inertia $I_{\alpha\beta}$ through [42]

$$Q_{\alpha\beta}=-3\,I_{\alpha\beta}+\varepsilon_{\alpha\beta}\,I_{\gamma\gamma}\,.$$

Slowly rotating fluid spheres are symmetric about the axis of rotation and $I_{\gamma\gamma}=0$ so that

$$Q_{\alpha\beta}=-3\,I_{\alpha\beta}\,.$$

In accordance with most authors we define the quadrupole moment Q to be

$Q=$ (coefficient of $-G\,r^{-3}\,P_2(\cos\vartheta)$ term in Newtonian potential)

(see however [52] where double this quantity is defined to be the quadrupole moment). Q is then related to I_{zz} – if the z-axis is the axis of rotation – by

$$Q=\tfrac{1}{2}\,Q_{zz}=-\tfrac{3}{2}\,I_{zz}\,.$$

For an incompressible fluid shere one obtains

$$I_{zz}=\frac{5}{8\,\pi}\,\frac{\Omega^2}{G\,\varrho}\,I$$

and for a polytrope ($p\sim\varrho^2$)

$$I_{zz}=\frac{\pi}{12}\,\frac{15-\pi^2}{\pi-6}\,\frac{\Omega^2}{G\,\varrho_c}$$

where ϱ_c is the central density of the star. In Table 4.2 we give computed values of Q/I for two different equations of state.

Table 4.2. Quadrupole moments of slowly rotating neutron stars for EOS 1 (a) and EOS 3 (b). The centrifugal forces have been treated in the Newtonian theory of gravitation. ϱ_c is the central density, I_N the Newtonian moment of inertia. Q the quadrupole moment as defined in the text for $\Omega = 300\ \mathrm{sec}^{-1}$, and $\Omega_c = (G\,M/R^3)^{1/2}$ is the critical angular frequency. Q scales as Ω^2.

	$\varrho_c/10^{15}$ g cm^{-3}	$I_N/10^{44}$ g cm^2	$10^3\,Q/I_N$	$\Omega_c/10^4$ sec^{-1}
a	0.35	7.04	1.09	0.59
	0.44	11.1	0.70	0.70
	0.53	14.9	0.54	0.79
	0.64	17.9	0.40	0.87
	0.74	20.0	0.31	0.94
	0.98	21.7	0.22	1.06
	1.24	21.3	0.18	1.17
	1.71	19.0	0.14	1.30
b	0.34	1.30	1.41	0.35
	0.43	2.10	1.03	0.50
	0.52	3.02	0.79	0.62
	0.61	3.98	0.62	0.71
	0.70	4.90	0.51	0.80
	0.89	5.97	0.35	1.00
	1.09	7.60	0.26	1.05
	1.41	8.44	0.19	1.19
	1.76	8.59	0.13	1.30
	2.26	8.22	0.10	1.42

Appendix A

We give here in more detail properties the different equations of state used to construct neutron star models. Both ε and P are always in MeV · (fm)$^{-3}$ and the particle density is in fm^{-3}. In the low density regime all equations of state (EOS) coincide and an analytic fit up to the neutron drip line is given by

$$n \leqq 2.6\times10^{-8},$$
$$\varepsilon = -2.31\times10^{-8}\,n/n_0 + P_0/0.48\,(n/n_0)^{1.48},$$
$$P = P_0\,(n/n_0)^{1.48}$$

with $n_0 = 2.45\times10^{-9}$ and $P_0 = 1.12\times10^{-10}$,

$$2.6\times10^{-8} \leqq n \leqq 2.63\times10^{-4},$$
$$\varepsilon = -11.8\times10^{-6}\,n/n_0 + P_0/0.30\,(n/n_0)^{1.30},$$
$$P = P_0\,(n/n_0)^{1.30}$$

with $n_0 = 1.22\times10^{-6}$ and $P_0 = 5.99\times10^{-7}$.

Between ϱ_2 and ϱ_3 our equation of state reads (EOS 1)

$$2.63\times10^{-4} \leqq n \leqq 3.4\times10^{-2},$$
$$\varepsilon = -0.5712\,n^{2/3} + 11.150\,n - 94.1997\,n^{4/3} + 485.5055\,n^{5/3} - 1018.0457\,n^2 + 1948.7326\,n^{8/3},$$
$$P = 0.1904\,n^{2/3} - 31.3999\,n^{4/3} + 323.6703\,n^{5/3} - 1018.0457\,n^2 + 3247.8876\,n^{8/3}.$$

(EOS 2) by Hohlinde et al.[30] and (EOS 3 a) Arponen[31] and (3 b) (Kälman) have instead

$$1.9\times10^{-4} \leqq n \leqq 0.09,$$
$$\varepsilon = -0.3475\,n^{2/3} + 6.0775\,n - 47.2697\,n^{4/3} + 283.5827\,n^{5/3} - 467.4328\,n^2 + 560.2093\,n^{8/3},$$
$$P = 0.1479\,n^{2/3} - 26.5511\,n^{4/3} + 283.5133\,n^{5/3} - 698.3886\,n^2 - 80.4885\,n^{10/3}.$$

The influence of the relativistic electrons and the Coulomb lattice of nuclei impose a more complicated equation of state in this region up to the phase transition into the homogeneous matter, as might be expected for a pure neutron gas.

In the high density regime where the nuclei have disappeared we have for

EOS 1:

$$n \geqq 3.4\times10^{-2},$$
$$\varepsilon = 77.5313\,n^{5/3} - 255.5201\,n^2 + 752.7546\,n^{8/3},$$
$$P = 23.5861\,n^{5/3} - 148.6313\,n^2 + 1037.8935\,n^{8/3}.$$

(As can be seen from this analytic fit the pressure P in this region has slightly other coefficients as would be derived from ε directly.)

EOS 2:

$$E/N = 8.59\,k\,f^2 - 2.80\,k\,f^3 + 0.15\,k\,f^5 + 0.06\,k\,f^7$$

(ε and P are calculated in the way discussed in § 2. We used this equation down to $n = 9\times10^{-3}$ for neutron star calculation.)

EOS 3 a (Arponen):

$$n \geqq 0.09$$
$$\varepsilon = 105.256\,n^{5/3} + 1.009\,n - 219.1143\,n^2 + 377.6837\,n^{8/3} - 80.4885\,n^{10/3}$$
$$P \geqq 39.4849\,n^{5/3} - 139.2263\,n^2 + 604.3449\,n^{8/3} - 247.8594\,n^{10/3}$$

EOS 3 b (Kälman):

$$n = 0.013$$
$$\varepsilon = (0.0485\,n^2 + 0.176\,n^3 + 0.0070\,n)\,m_N\,c^2$$
$$P = 133\,n^{5/3}(0.36 + 1.47\,n + 0.188\,n^2 + 0.433\,n^3) - 0.0095.$$

EOS 4 has been described in the text and

EOS 5 reads for

$$n \geqq 0.842$$
$$\varepsilon = 95.939\,n - 66.1172\,n^{4/3} + 1618.7501\,n^{5/3} - 1300.7847\,n^2 + 270.2629\,n^{8/3},$$
$$P = 286.8027\,n^{5/3} - 535.4005\,n^2 + 253.4029\,n^{8/3} + 9.3255\,n^{10/3}.$$

We used Pandharipande's equation of state A which has a phase transition at $P = 1.17$ MeV/fm^3, where n jumps from 0.842 to 0.12. Below this density we used EOS 3.

[1] For an excellent review of both observations and theoretical models of pulsars see D. Ter. Haar, Physics Letters **3 C**, 57 [1972].

[2] G. Giacconi, VI. Texas-Symposion, to be published in Ann. Proc. N. Y. Acad. Sci. (Dec. 1972), and Physics Today, May 1973; R. A. Sunayew, N. I. Shakura, Astr. Astroph. **24**, 337 [1973].

[3] The crab nebula, I. A. U. Symp. No. **46**, D. Reidel, Dordrecht 1970.

[4] M. A. Ruderman, Phys. Rev. Lett. **27**, 1306 [1971]; R. O. Mueller, A. R. P. Rau, and L. Spruch, Nature Phys. Sci. **235**, 31 [1971]; B. B. Kadomtsev and V. Kudryavtsey, J. Exp. Theor. Phys. **13**, 1, 42 [1971], J. Exp. Theor. Phys. **35**, 76 [1972]; V. I. Ginzburg and V. V. Usov, J. Exp. Theor. Phys. **15**, 196 [1972]; J. I. Kaplan and M. L. Glasser, Phys. Rev. Lett. **28**, 1077 [1972].

[5] E. E. Salpeter, Astrophys. J. **134**, 669 [1961].

[6] G. Baym, C. Pethick, and P. Sutherland, Astrophys. J. **170**, 299 [1971].

[7] J. R. Buchler and Z. Bakarat, Phys. Rev. Lett. **27**, 48 [1971]; Astrophys. Lett. **7**, 167 [1971].

[8] W. D. Langer, L. C. Rosen, J. M. Cohen, and A. G. W. Cameron, Astrophys. Space Sci. **5**, 259 [1969].

[9] H. A. Bethe, G. Börner, and K. Sato, Astron. Astroph. **7**, 279 [1969].

[10] G. Baym, H. A. Bethe, and C. Pethick, Nucl. Phys. **A 175**, 225 [1971].

[11] J. R. Buchler and L. Ingber, Nucl. Phys. **A 170**, 1 [1971].

[12] P. J. Siemens and V. R. Pandharipande, Nucl. Phys. **A 173**, 561 [1971].

[13] M. Miller, C. W. Woo, J. W. Clark, and W. J. Terlow, Nucl. Phys. **A 184**, 1 [1972].

[14] H. Y. Chiu and E. E. Salpeter, Phys. Rev. Lett. **12**, 413 [1964]; J. N. Bahcall and R. A. Wolf, Phys. Rev. **140**, B 1452 [1965]; A. Finzi and R. A. Wolf, Astrophys. J. **153**, 835 [1968].

[15] R. F. Sawyer, Phys. Rev. Lett. **29**, 382 [1972]; D. J. Scalapino, Phys. Rev. Lett. **29**, 386 [1972]; J. Kogut and J. T. Manassah, Phys. Lett. **A 41**, 129 [1972]; A. B. Migdal, Phys. Rev. Lett. **31**, 257 [1973].

[16] H. Heintzmann and J. Nitsch, Astron. Astroph. **21**, 291 [1972].

[17] R. L. Kinzer, R. C. Noggle, N. Seeman, and G. H. Share, Nature London **229**, 187 [1971]; W. Kunkel, P. Osmer, M. Smith, A. Hoag, D. Schroeder, W. A. Hiltner, H. Bradt, S. Rappaport, and H. W. Schnopper, Ap. J. Lett. **161**, L 173 [1970].

[18] L. Davis and M. Goldstein, Astrophys. J. **159**, L 81 [1969].

[19] P. Goldreich and W. H. Julian, Astrophys. J. **157**, 869 [1969].

[20] F. Meyer, in: Einheit und Vielheit (v. Weizsäcker Geburtstagsband), ed. E. Scheibe und G. Süßmann, Vandenhoek and Rupprecht, Göttingen 1973.

[21] N. Itoh, Progr. Theor. Phys. **42**, 1478 [1969]; C. H. Yang and J. W. Clark, Nucl. Phys. **A 174**, 49 [1971]; T. Takatsuka and R. Tamagaki, Progr. Theor. Phys. **46**, 114 [1971]; R. W. Richardson, Phys. Rev. **D 5**, 1883 [1972]; E. Østgaard, Z. Physik **243**, 79 [1971]; E. Krotscheck, Z. Physik **251**, 135 [1972].

[22] N. C. Chao, J. W. Clark, and C. H. Yang, Nucl. Phys. **A 179**, 320 [1972]; C. H. Yang and J. W. Clark, Lett. Nuovo Cim. **4**, 969 [1972].

[23] J. W. Clark and N. C. Chao, Nature Phys. Sci. **236**, 37 [1972]; V. Canuto, S. M. Chitre, L. Nosanov, and Parish, Ann. of the Proceedings of the N. Y. Acad. of Sci., 6th Texas Symposium on Relativistic Astrophysics, New York, Dec. 1972; J. W. Clark, Solid stars = Fact or Fictition Proc. Sympos. on: Present Status and Novel Developments in the Many-Body-Problem, Rome 1972 to be published in the Proceedings.

[24] R. A. Weiss and A. G. W. Cameron, Canad. J. Phys. **47**, 2171 [1969].

[25] J. S. Levinger and L. M. Simmons, Phys. Rev. **124**, 916 [1961].

[26] W. D. Myers and W. J. Swiatecki, Nucl. Phys. **81**, 1 [1966]; Ann. Phys. (N. Y.) **55**, 395 [1969].

[26a] R. G. Seyler and C. H. Blanchard, Phys. Rev. **124**, 227 [1961]; Phys. Rev. **131**, 355 [1963].

[26b] S. Ludwig, H. v. Groote, E. Hilf, A. G. W. Cameron, and T. Truran, Nucl. Phys. **A 203**, 627 [1973].

[27] A. G. W. Cameron, Chalk River Rept. (March, 1957).

[28] M. F. El Eid, K. Koebke, and E. Hilf, to be published.

[29] H. von Groote, M. F. El Eid, and E. Hilf, to be published.

[30] K. Hohlinde, R. Alzetta, and K. Erkelenz, Nucl. Phys. **A 194**, 161 [1972].

[31] J. Arponen, Nucl. Phys. **A 191**, 257 [1972].

[32] G. Kälman, preprint; Kälman's work is based on recent work by S. Babu and G. E. Brown, Ann. Phys. N.Y. **78**, 1 [1973], and O. Sjöberg, ibid. 39.

[33] R. K. Cole, jr., Phys. Rev. **155**, II, 114 [1967].

[34] Ya. B. Zeld'ovich, Sov. Phys. JEPT **14**, 1143 [1962].

[35] H. Heintzmann, Astron. Astroph. **5**, 488 [1970].

[36] V. R. Pandharipande, Nucl. Phys. **A 178**, 561 [1971].

[37] M. L. Libby and F. J. Thomas, Phys. Lett. **30**, 88 [1969].

[38] H. Heintzmann and W. Hillebrandt, Astron. Astroph. **7**, 443 [1970].

[39] H. Heintzmann, Astron. Astroph. **5**, 488 [1970]; H. Heintzmann, in: Proceedings of the international school of physics Enrico Fermi, 47, Academic Press, New York 1971.

[40] P. Jordan, Schwerkraft und Weltall (Vieweg, Braunschweig 1955), Rev. Mod. Phys. **34**, 596 [1962]; C. Brans and R. H. Dicke, Phys. Rev. **124**, 925 [1961]; A. Salmona, Phys. Rev. **154**, 1218 [1967]; G. S. Saakyan and M. A. Mratsakanyan, Astrophys. **5**, 271 [1970]; R. Ruffini and J. A. Wheeler, Cosmology from Space Platform, ESRO Book SP 52, Paris 1971.

[41] W. Hillebrandt and H. Heintzmann, GRG, in press.

[42] L. D. Landau and E. M. Lifshitz, Statistische Physik, Akademie Verlag, Berlin 1966.

[43] J. M. Cohen, Astrophys. Space Sci. **6**, 263 [1970]; F. B. Hartle and K. S. Thorne, Astrophys. J. **153**, 807 [1968].

[44] F. Drake, VI Texas Symp. see Ref. 2; P. E. Reichley, ibid. and Nature Phys. Sci. **234**, 48 [1971].

[45] J. Nelson, R. Hills, D. Cudaback, and J. Wampler, Astrophys. J. **161**, L 235 [1970]; P. E. Boynton, E. J. Groth, D. P. Hutchinson, G. P. Nanos, R. B. Partridge, and D. T. Wilkinson, Astrophys. J. **175**, 217 [1972].

[46] M. A. Ruderman, Nature London **223**, 597 [1969]; G. Baym and D. Pines, Ann. Phys. **66**, 816 [1971]; Shaham, VI. Texas Symp. see Ref. 2.

[47] H. Heintzmann, W. Hillebrandt, E. Krotscheck, and W. Kundt, VI. Texas Symp., N. Y., Ann. Phys. (N. Y.) **81**, 625 [1973].

[48] H. Heintzmann, W. Kundt, and E. Schrüfer, Inside rotating neutron stars, Cern preprint TH 1604 (1972), submitted to Astron. and Astrophys.

[49] K. S. Thorne, in "Proc. of the Intern. School of Phys. Enrico Fermi", Academic Press, New York **47** (1971).

[50] P. Goldreich, Astrophys. J. **160**, L 11 [1970].

[51] S. Chandrasekhar, Phys. Rev. Lett. **24**, 611 [1970].